Copyright © 2012 Tech Science Press CMES, vol.87, no.4, pp.271-305, 2012

Thin Plate Bending Analysis and Treatment of Material Discontinuities Using the Generalised RKP-FSM

M. Khezri[1], Z. Vrcelj[1] and M.A. Bradford[1,2]

Abstract: A finite strip method (FSM) utilising the generalised reproducing kernel particle method (RKPM) [Behzadan, Shodja, and Khezri (2011)] is developed for the bending analysis of thin plates. In this innovative approach, the spline functions in the conventional spline finite strip method (SFSM) are replaced with generalised RKPM 1-D shape functions in the longitudinal direction, while the transverse cubic functions which are used in the conventional formulations are retained. Since the generalised RKPM is one of the class of meshfree methods which deal efficiently with derivative-type essential boundary conditions, its introduction in the FSM is beneficial for solving boundary value problems such as the bending of thin plates in which a number of essential boundary conditions can include first derivatives of the displacement function. In this paper, the formulation for the generalised RKP-FSM is derived for the analysis of thin plates, and its accuracy and convergence are examined through a series of numerical studies. Moreover, by modifying the concept of the augmented corrected collocation method [Shodja, Khezri, Hashemian, and Behzadan (2010)] a new feature is added to the conventional SFSM and the generalised RKP-FSM which allows for the exact treatment of material discontinuities in bending analysis. Oscillatory behaviour of solutions near the interface of material discontinuities due to Gibb's phenomenon is successfully eliminated in both methods.

Keywords: generalised RKP-FSM, spline finite strip method, thin plate bending, material discontinuities, meshfree methods.

1 Introduction

It is without question that the finite element method (FEM) is the most frequently-used and dominant technique for finding approximate solutions of differential and

[1] Centre for Infrastructure Engineering and Safety, School of Civil and Environmental Engineering, The University of New South Wales, UNSW Sydney, NSW 2052, Australia.

[2] Corresponding author. Tel: +61 2 9385 5014; Fax: +61 2 9385 9747; E-mail: M.Bradford@unsw.edu.au (M.A. Bradford)

integral equations in engineering science. Since its introduction in the middle of the last century, it has been widely-applied in different engineering fields and specifically in the field of computational mechanics. However, like any other method, the FEM has its own specific drawbacks and disadvantages which limit or excessively complicate its application in certain problems [Khezri, Hashemian, and Shodja (2009)]. Different numerical methods have been developed and applied to treat and rectify these drawbacks, the main two of which are meshfree methods and finite strip methods. Both of these two classes of numerical techniques have some advantages over the conventional FEM, and these beneficial characteristics are the main reason for their continuing development. Among the major advantages are lower computational costs and mesh-dependency elimination, which are the most common benefits of finite strip and meshfree methods.

While the most recognised advantages of the FSM over the conventional FEM are its reduced computer storage and the time required to model the problem [Cheung, Li, and Chidiac (1996)], meshfree methods have advantages that are more apparent when dealing with problems in which the meshing characteristics of the FEM make its application expensive or inefficient, i.e. for large deformations, complex geometry, fracture mechanics and singular or discontinuities fields [Liu and Gu (2005)], [Erkmen and Bradford (2010a,b)]. A method that can successfully combine the aforementioned advantages of these two classes of methods, while avoiding some of their drawbacks, seems to hold some promise. In this paper, this concept is explored by enriching the FSM using the generalised RKPM as the approximation tool in the longitudinal direction. A brief review of the related developments and the advancements in the FSM and the RKPM is crucial to grasp the implemented concept, and to gain a deeper insight of the methodology presented. To this end, the background of FSM and RKPM is reviewed briefly in the following.

The well-established semi-analytical FSM, in deference to the "exact" formulation of Wittrick and Williams (1970), was first proposed as an extension of the FEM for the analysis of isotropic and orthotropic plates of variable thickness with two opposite simply-supported ends [Cheung (1968)]. Since then, the technique has been advanced by several researchers. Prominent among these developments was the introduction of the spline finite strip method (SFSM), which significantly improved the method's versatility in modelling a comprehensive range of structures with different boundary conditions [Cheung and Fan (1983)]. The semi-analytical FSM and the SFSM, as the two main branches of FSM, are different in their nature of approximation in the longitudinal direction. Other variations of FSM adopt different approximation schemes not only in the longitudinal direction but also in the transverse direction. For example, Azhari, Hoshdar, and Bradford (2000) augmented the spline FSM by using Legendre bubble functions in the transverse di-

rection. In 2003, Liew, Zou, and Rajendran proposed a new FSM formulation by including the RKPM as the approximation tool in the transverse direction. Their work could be considered as the first hybrid method obtained by combining the conventional RKPM and the FSM.

The beginnings of meshfree methods appear to date back to 1976, when the smooth particle hydrodynamic method (SPH) was first-developed for application in the field of astrophysics [Lucy (1977)]. The major shortcoming of the SPH was that it fails to create accurate results in the vicinity of the boundaries or when the number of particles used is small [Liu, Jun, Li, Adee, and Belytschko (1995)]. In 1995, Liu, Jun, Li, Adee, and Belytschko employed a correction function in the reproduction formula of the SPH method to rectify the problem in the vicinity of the boundaries. In the formulation they developed, which is called the RKPM, the fluctuations that occurred in the results were eliminated, and the accuracy of the amplitude of the results obtained was also improved significantly. Despite being helpful for different kinds of problems, the conventional RKPM has a drawback in dealing with the problems that involve derivatives of the field functions as the essential boundary conditions (EBCs). When Shodja and Hashemian (2007) were studying beam-column problems, they found it difficult to enforce the EBCs involving the derivatives of the field variable. To remedy this problem, they incorporated the first derivative of the function in the reproduction formula of the RKPM and named the evolved method the Gradient RKPM [Hashemian and Shodja (2008)]. In a further development, Behzadan, Shodja and Khezri (2011) generalised the RKPM technique in a way for which any order of derivatives of the function could be incorporated in formulations. In the present study, the one-dimensional formulation of the generalised RKPM has been adopted as the approximation tool in the longitudinal direction.

In parallel with the RKPM development, several other notable meshfree methods have been proposed in the past couple of decades. Nayroles, Touzot, and Villon (1992) presented the Diffuse Element Method (DEM) as a generalization of the FEM by removing some of the limitations of the FEM approximation. Their work was based on the application of moving least square methods which was originally proposed by Lancaster and Salkauskas (1981) as a smoothing and interpolation tool for scattered data. Later, Belytschko, Lu, and Gu (1994) presented the Element Free Galerkin Method (EFGM) by using moving least squares interpolations for constructing the trial and test function of the variational principle, and for the first time applied it in elasticity and heat conduction problems. Durate and Oden (1996), after showing that the moving least squares functions (MLSF) constitutes a partition of unity, presented a new meshless method called an $h-p$ cloud by multiplying a partition of unity; MLSF by a proper class of functions. Melnek and Babuška

(1996) developed the Partition of Unity Finite Element Method (PUFEM) for the solution of differential equations. Zhu, Zhang, and Atluri (1998a, b) introduced the Local Boundary Integral Equation (LBIE) method and successfully applied it in the analysis of non-linear problems and problems with non-homogeneous domains. At the same time, Atluri and Zhu (1998) developed the Meshless Local Petrov-Galerkin (MLPG) method, which was based on the local weak forms unlike the RKPM and EFGM which depend on the global weak forms. Later, they applied their method for solving problems in elasto-statics [Atluri and Zhu (2000)]. A comprehensive review of the variations of MLPG methods is presented by Atluri and Shen (2002a, b).

One of the most commonly emphasised features of meshfree methods is that the shape functions with any desired order of smoothness can be constructed easily by the employment of appropriate window functions and basis functions. As a consequence and unlike the FEM, no further post-processing is required in the solution of Boundary Value Problems (BVPs) in solid mechanics for obtaining smooth stress fields [Shodja, Khezri, Hashemian, and Behzadan (2010)]. Although this feature is quite helpful in the majority of cases, it can also be problematic, e.g. for the analysis of plate structures with step changes in the thickness or plates with discontinuous material properties. In general, this issue is due to the inherent excessive continuity, and special measures should be taken to model the condition near the break point accurately. The very same problem could be encountered in the analyses using SFSM due to its excessive continuity in the longitudinal direction. While the treatment of material discontinuities in the field of meshfree methods have always been of particular interest, in the context of the FSM the proposed methodologies for this purpose are limited, and when attempted in the past with continuous shape functions, the proper conditions have not been met [Dawe, and Tan (2002)]. Cheung, Au, and Zhang (1998) considered the in-plane static analysis of plates with step rigidity changes and proposed a suitable displacement field satisfying the required C^0 continuity as the solution. Later, the same authors proposed a FSM approach satisfying the required C^1 continuity for free vibration and buckling analysis of plates with abrupt changes in thickness and complex support conditions [Cheung, Au, and Zhang (2000)]. In a different approach, Dawe and Tan (1999) suggested local refinement of the splines in the vicinity of breakpoints as a solution to the problem. Although their approach gives satisfactory results for the out-of-plane vibration and buckling of single stepped plates, it is predictable that for the static analysis of these plates, particularly when the stress distribution is required in the vicinity of the abrupt changes, the results obtained will not be satisfactory. Thus, they proposed an improved SFSM in which the continuity order is reduced at the breakpoint by placing two section knots at the same coordinate

[Dawe and Tan (2002)].

In the present research, the authors seek to enrich the SFSM by introducing formulations for the treatment of material discontinuities commonly adopted by meshfree methods. Nevertheless, the treatment of these conditions in meshfree methods, due to their higher order continuity, is often accompanied by additional complications. As a result, a substantial amount of research has been devoted to this topic since the introduction of meshfree methods. Cordes and Moran's (1996) study was one of the first to tackle the problem by separate discretisation of the parts in the problem utilizing the moving least squares (MLS). In order to enforce continuity of the displacements at the interface, they employed the method of Lagrange multipliers. Krongauz and Belytschko (1998) and Masuda and Noguchi (2006), in a similar approach, modelled the discontinuity problem utilising special shape functions with jump discontinuity across the interface. In the context of the EFGM, Kawashima and Noguchi (2000) separately discretised each part and then enforced the continuity condition at the interface by means of a penalty method. Using the MLPG method, Li, Shen, Han, and Atluri (2003) proposed an accurate and efficient methodology for the treatment of singularities and material discontinuities in 3-D elasticity. Shodja, Khezri, Hashemian, and Behzadan (2010) considered the same problem in the context of the RKPM, and proposed an augmented collocation method for the treatment of material discontinuity. In this study, the same augmented collocation method for the treatment of material discontinuity has been incorporated in the proposed RKP-FSM to model bending of bi-material plates. By adopting the same concept, the SFSM has also been modified to enable modelling of material discontinuities or abrupt changes in the thickness of plates subjected to bending.

The outline of this paper is as follows. In Section 2, the new generalised RKP-FSM is introduced. Section 3 is devoted to describing the thin plate bending analysis and the assumed displacement function in the context of the new proposed FSM (RKP-FSM). Section 4 briefly presents the applied method for enforcement of the essential boundary conditions. In Section 5, the concept utilised and the modified method for the treatment of material discontinuities is presented, while Section 6 presents a number of numerical examples illustrating the efficacy of the new proposed RKP-FSM and an example of bi-material plate bending analysis using the developed method is also presented. Section 7 concludes the paper.

2 Generalised RKP-FSM

In the variations of the FSM, the rudimentary idea is to construct an approximation of the field variables by combining two separate longitudinal and transverse approximations [Liew, Zou, and Rajendran (2003)]. Accordingly in the usual SFSM,

the field variable is derived by multiplication of two separate approximations: one using spline functions in the longitudinal direction and the other utilising cubic polynomials in the transverse direction [Vrcelj, and Bradford (2010)]. Herein, the same concept is incorporated, but the generalised RKPM approximation has been applied in the longitudinal direction by replacing the conventional spline functions. Using the aforementioned scheme of approximation, a given function $u(x,y)$ in a two-dimensional domain Ω, with the boundary Γ, can be expressed as

$$\hat{u}(x,y) = f^R(x)\ g(y), \tag{1}$$

in which $\hat{u}(x,y)$ is the approximated longitudinal function obtained via the generalised RKPM, and $g(y)$ stands for the same approximation of the conventional SFSM in the transverse direction using cubic polynomial shape functions. The new proposed method can be considered as a hybrid method which amalgamates the positive features of both meshfree and FSMs. The following two subsections provide the details of the method and the structure of the approximation.

2.1 Generalised RKPM approximation in the longitudinal direction

In the generalised RKPM, a given function $f(x)$ in a one-dimensional domain ℓ, can be expressed in terms of the functions and its derivatives by the reproducing formula as [Behzadan, Shodja, and Khezri (2011)], [Liu, Jun, Li, Adee, and Belytschko (1995)]:

$$f^R(x) = \sum_{\eta=0}^{k} \int_{\ell} \frac{1}{a(\xi)} C^{[\eta]}(x; x-\xi)\, \varphi\left(\frac{|x-\xi|}{a(\xi)}\right) f_{,\eta}(\xi)\, \mathrm{d}\ell, \tag{2}$$

where $f^R(x)$ is the reproduced function, φ is the kernel function, $|\cdot|$ is the absolute value for the distance between x and ξ, and k is the highest order of the considered derivative which is incorporated in the reproduction formula. In equation (2), a is the dilation parameter, and $f_{,k}(\ \xi\ )$ is defined as

$$f_{,0}(\xi) = f(\xi), \qquad f_{,\eta}(\xi) = \frac{\mathrm{d}^{\eta} f(\xi)}{\mathrm{d}\xi^{\eta}}; \quad \eta = 1,2,...,k. \tag{3}$$

Also,

$$C^{[\eta]}(x; x-\xi) = \frac{\mathrm{d}^{\eta} C(x; x-\xi)}{\mathrm{d}\xi^{\eta}} \qquad \forall \eta, \quad \eta \le k \tag{4}$$

are correction functions which are derived by differentiating the reference correction function $C(x;\ x-\xi)$. The reference correction function can be stated as a linear

combination of polynomial basis functions given as

$$C(x;x-\xi)=\sum_{i=0}^{m} b_i(x)(x-\xi)^i. \tag{5}$$

In equation (5) above, m is the maximum order of the polynomial function which can be reproduced exactly, and $b_i(x)$ is a set of unknown coefficients which can be determined by the completeness condition. Setting

$$\mathbf{p}(x-\xi)=\begin{bmatrix}1 & (x-\xi) & (x-\xi)^2 & \dots & (x-\xi)^i & \dots & (x-\xi)^m\end{bmatrix}^{\mathrm{T}} \tag{6}$$

and

$$\mathbf{b}(x)=\begin{bmatrix}b_0(x) & b_1(x) & b_2(x) & \dots & b_i(x) & \dots & b_m(x)\end{bmatrix}^{\mathrm{T}} \tag{7}$$

results in the reference correction function being restated using matrix notation as

$$C(x;x-\xi)=\mathbf{p}^{\mathrm{T}}(x-\xi)\mathbf{b}(x). \tag{8}$$

The coefficients vector $\mathbf{b}(x)$ should be determined such that the reproduction formula in equation (2) exactly reproduces the polynomials with the required order m. Accordingly, by imposing the completeness condition, these coefficients can be calculated by

$$\mathbf{b}(x)=\mathbf{M}^{-1}(x)\mathbf{H}(0), \tag{9}$$

in which $\mathbf{M}(x)$ is the moment matrix. The required steps for the derivation of the moment matrix are illustrated later in this section.

It is evident that equation (2) is a continuous reproducing kernel approximation, and the considered domain must be discretised using a set of particles to find an approximate solution. By applying trapezoidal rule, the equation becomes

$$f^R(x)=\sum_{\eta=0}^{k}\sum_{I=1}^{NP} C^{[\eta]}(x;x-\xi_I)\,\varphi\left(\frac{|x-\xi_I|}{a_I}\right) f_{,\eta}(\xi)|_{\xi=\xi_I}\,\Delta x_I, \tag{10}$$

where NP is the number of particles, and Δx_I is the length associated with particle. Utilizing the discretisation scheme, the moment matrix arrays can be determined using the relation [Behzadan, Shodja, and Khezri (2011)]

$\forall\ 1\le i,j\le m+1$:

$$M_{j,i}(x)=\sum_{\eta=0}^{k} S_{j-1,\eta}\,S_{i-1,\eta}\,\frac{(i-1)!\,(j-1)!}{(i-1-\eta)!\,(j-1-\eta)!}\,m_{i+j-2\eta-2} \tag{11}$$

where $S_{\alpha,\beta}$ is an index and is set to be

$$S_{\alpha,\beta} = \begin{cases} 1 & \beta \leq \alpha \\ 0 & \beta > \alpha \end{cases} \tag{12}$$

and

$$\forall \theta \in \mathrm{Z} \qquad m_\theta(x) = \begin{cases} \sum_{I=1}^{NP} (x - x_I)^\theta \, \phi\left(\frac{x-x_I}{a_I}\right) \Delta x_I & \theta \geq 0 \\ 1 & \theta < 0 \end{cases}. \tag{13}$$

In equation (13), ϕ is the kernel function, also known as the window function. Different window function choices are available for adoption as the kernel of the method. Some of these functions have been examined and studied by Donning and Liu (1998). In the present research, the following window function has been used [Han and Meng (2001)]:

$$\phi(x) = \begin{cases} \left(1 - x^2\right)^9 & \text{if } |x| \leq 1 \\ 0 & \text{otherwise} \end{cases}. \tag{14}$$

Since all the required functions in equation (10) can be evaluated numerically using relations (5)-(13), equation (10) can be restated as

$$f^R(x) = \sum_{\eta=0}^{k} \sum_{I=1}^{NP} \psi_I^{[\eta]}(x) \; f_{,\eta}^I, \tag{15}$$

where

$$\psi_I^{[\eta]}(x) = C^{[\eta]}(x, x - x_I) \, \phi\left(\frac{x - x_I}{a_I}\right) \Delta x_I \tag{16}$$

and $\psi_I^{[\eta]}(x)$ are the particle I's associated shape functions. It is clear that the number of shape functions at each node is dependent on the order of the derivative considered in the reproducing formula. The shape functions obtained will be employed in the longitudinal direction to approximate the field variables considered. In the present study, only the first derivative of the function will be incorporated in the approximation function. Accordingly, by setting k= 1, two sets of functions will be constructed. Schematic views of these functions in an arbitrary domain with uniform discretisation scheme using 11 particles are presented in Figs. 1 and 2.

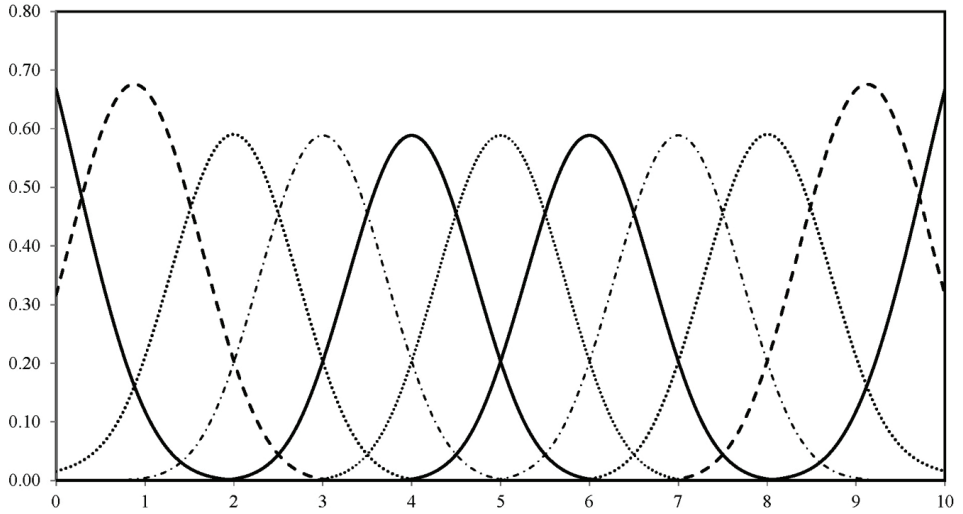

Figure 1: Generalised RKPM shape function associated with the function $\psi_I^{[0]}(x)$

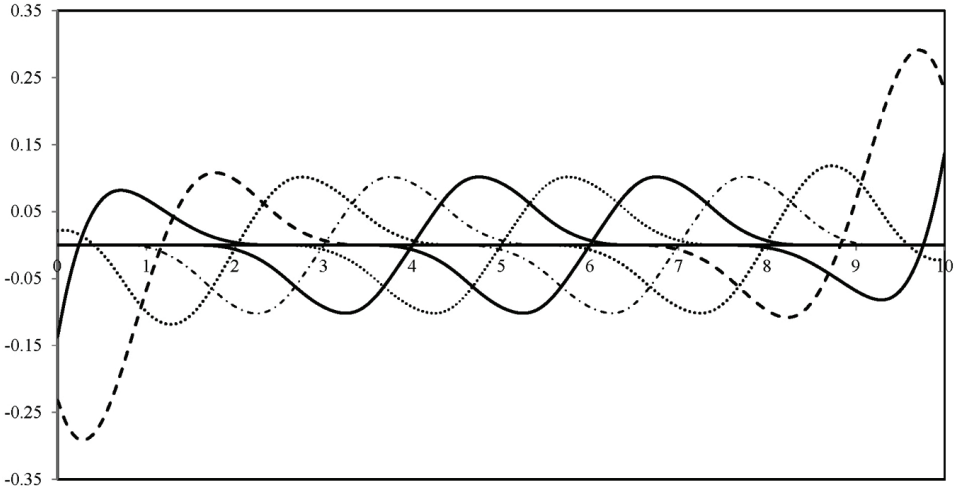

Figure 2: Generalised RKPM shape function associated with the first derivative of the function $\psi_I^{[1]}(x)$

2.2 Cubic polynomial interpolation in transverse direction

As in the conventional SFSM, a cubic polynomial interpolation will be adopted in the transverse direction. These shape function are [Vrcelj and Bradford (2008)]

$$\begin{cases} N_1 = 1 - 3\bar{y}^2 + 2\bar{y}^3 \\ N_2 = y\left(1 - 2\bar{y} + \bar{y}^2\right) \\ N_3 = \left(3\bar{y}^2 - 2\bar{y}^3\right) \\ N_4 = y\left(\bar{y}^2 - \bar{y}\right), \end{cases} \quad ; \qquad \bar{y} = \frac{y}{b} \tag{17}$$

in which b is the width of the strip. Of course, the shape functions presented are for lower order (LO2) and higher order strips such as (HO2) and (HO3), or strips with augmentation of bubble functions could be constructed by replacing and adding proper shape functions [Azhari, Hoshdar, and Bradford (2000)].

3 Displacement function and thin plate bending

Consider a thin rectangular plate of length L, width W and thickness t. Based on commonly adopted classifications, a plate would be categorised as a *thin plate* if $8..10 \leq (L/t,\ W/t) \leq 80..100$ [Ventsel and Krauthammer (2001)]. This general structural member is discretised in the transverse direction using n nodal lines, and in the longitudinal direction each nodal line is further segmented using m sections. In the conventional SFSM, two additional segments are placed at both ends of strips in order to fully define the B_3-spline functions along the length of the strip [Lau and Hancock (1996)]. In the proposed RKP-FSM, due to the application of a complete set of shape functions in the longitudinal direction, these additional segments are no longer required. Accordingly, the number of section knots, which equals m + 3 in the SFSM, would be reduced to m + 1. It is noteworthy that the number of additional segments is dependent on the type of spline function which is incorporated in the formulation, i.e. application of a B_5 -spline will require four additional outer segments [Dawe and Wang (1992)]. In fact, elimination of these additional segments is one of the features of the RKP-FSM. Appropriate modelling of the boundary conditions requires cumbersome amendment of outer spline functions, which is avoided in the new proposed method. General schematic discretisation patterns for the SFSM and the RKP-FSM are shown Fig. 3.

Based on the convergence criteria, a minimum of two degrees of freedom per nodal

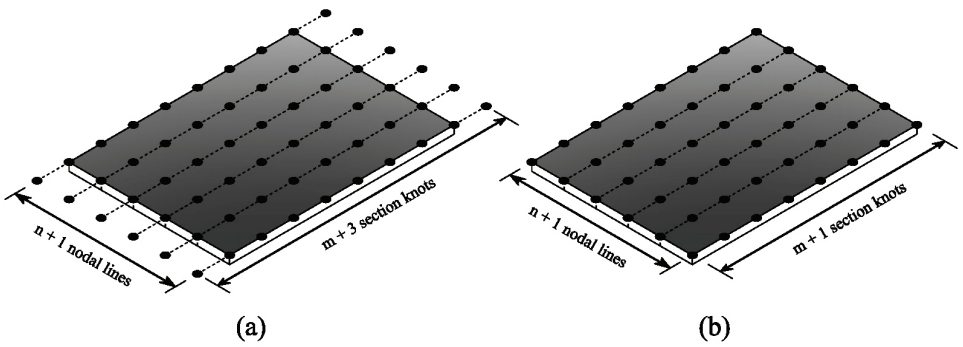

Figure 3: General discretisation schemes: (a) for SFSM; (b) for RKPM-FSM

line is necessary so that minimum compatibility conditions could be met for the deflection w and the rotation θ_y [Fan (1982)]. Accordingly, for the conventional SFSM, the deflection displacement function normal to the plane of the strips can be stated as the product of the B_3 - spline approximation in the longitudinal direction and the cubic polynomials in the transverse direction as

$$w = \begin{bmatrix} N_1 & N_2 & N_3 & N_4 \end{bmatrix} \begin{bmatrix} \Phi & & & \\ & \Phi & & \\ & & \Phi & \\ & & & \Phi \end{bmatrix} \begin{bmatrix} \mathbf{w}_i \\ \boldsymbol{\theta}_{iy} \\ \mathbf{w}_j \\ \boldsymbol{\theta}_{jy} \end{bmatrix} = \mathbf{N} \cdot \boldsymbol{\Phi} \cdot \boldsymbol{\delta}, \tag{18}$$

in which i and j are the indices for the nodal lines in each strip, and Φ is a row vector containing $m + 3$ B_3- spline functions given as

$$\boldsymbol{\Phi} = \begin{bmatrix} \varphi_{-1} & \varphi_0 & \varphi_1 & \ldots & \varphi_{m-1} & \varphi_m & \varphi_{m+1} \end{bmatrix}, \tag{19}$$

in which φ_i is the B_3-spline function and can be determined as presented by [Vrcelj and Bradford (2008)].

As was mentioned previously, in the proposed RKPM-FSM not only are the field variables included in the approximation equation, but also their first derivatives with respect to the longitudinal axis x. This means that in addition to the deflection w and the rotation θ_y, their derivatives with respect to the x axis $(w)_{,x}$ and $(\theta_y)_{,x}$ are also incorporated as nodal values. It is obvious that $(w)_{,x}$ is the rotation in the x direction and can be presented by θ_x. Hence, the displacement function for the RKP-FSM can be expressed as

$$w = \begin{bmatrix} N_1 & N_2 & N_3 & N_4 \end{bmatrix} \begin{bmatrix} \boldsymbol{\psi}^{[0]} & \boldsymbol{\psi}^{[1]} & & & & & & \\ & & \boldsymbol{\psi}^{[0]} & \boldsymbol{\psi}^{[1]} & & & & \\ & & & & \boldsymbol{\psi}^{[0]} & \boldsymbol{\psi}^{[1]} & & \\ & & & & & & \boldsymbol{\psi}^{[0]} & \boldsymbol{\psi}^{[1]} \end{bmatrix} \begin{bmatrix} \mathbf{w}_i \\ \boldsymbol{\theta}_{ix} \\ \boldsymbol{\theta}_{iy} \\ (\boldsymbol{\theta}_{iy})_{,x} \\ \mathbf{w}_j \\ \boldsymbol{\theta}_{jx} \\ \boldsymbol{\theta}_{jy} \\ (\boldsymbol{\theta}_{jy})_{,x} \end{bmatrix} = \mathbf{N}.\boldsymbol{\Psi}.\boldsymbol{\delta}, \tag{20}$$

where

$$\boldsymbol{\psi}^{[0]} = \begin{bmatrix} \psi_1^{[0]} & \psi_2^{[0]} & \ldots & \psi_{m+1}^{[0]} \end{bmatrix} \tag{21}$$

$$\boldsymbol{\psi}^{[1]} = \begin{bmatrix} \psi_1^{[1]} & \psi_2^{[1]} & \ldots & \psi_{m+1}^{[1]} \end{bmatrix} \tag{22}$$

$\boldsymbol{\psi}^{[0]}$ and $\boldsymbol{\psi}^{[1]}$ are the row vectors of the first and second type shape functions of the generalised RKPM, which can be determined using equation (16).

Now that the displacement functions for both methods have been illustrated, the aforementioned method can be progressed for undertaking a thin plate analysis. Since the thin plate bending analysis formulation for the SFSM has been extensively presented in the open literature, the derivation of the stiffness matrix and force vector utilising the RKP-FSM displacement function is presented only briefly herein.

Using equation (20), the state of strain in a rectangular plate in bending is described as

$$\boldsymbol{\varepsilon} = \begin{Bmatrix} -\frac{\partial^2 w}{\partial x^2} \\ -\frac{\partial^2 w}{\partial y^2} \\ 2\frac{\partial^2 w}{\partial x \partial y} \end{Bmatrix} = \begin{bmatrix} -\frac{\mathrm{d}^2 \mathbf{N}}{\mathrm{d}x^2} & \underset{\sim}{0} & \underset{\sim}{0} \\ \underset{\sim}{0} & -\mathbf{N} & \underset{\sim}{0} \\ \underset{\sim}{0} & \underset{\sim}{0} & 2\frac{\mathrm{d}\mathbf{N}}{\mathrm{d}x} \end{bmatrix} \begin{bmatrix} \boldsymbol{\Psi} \\ \frac{\mathrm{d}^2 \boldsymbol{\Psi}}{\mathrm{d}y^2} \\ \frac{\mathrm{d}\boldsymbol{\Psi}}{\mathrm{d}x} \end{bmatrix} \begin{bmatrix} \mathbf{w}_i \\ \boldsymbol{\theta}_{ix} \\ \boldsymbol{\theta}_{iy} \\ (\boldsymbol{\theta}_{iy})_{,x} \\ \mathbf{w}_j \\ \boldsymbol{\theta}_{jx} \\ \boldsymbol{\theta}_{jy} \\ (\boldsymbol{\theta}_{jy})_{,x} \end{bmatrix} = \mathbf{B} \cdot \boldsymbol{\delta}. \tag{23}$$

By adopting linear elasticity, the strain-stress relationship for a thin orthotropic plate can be stated as

$$\boldsymbol{\sigma} = \begin{Bmatrix} M_x \\ M_y \\ M_{xy} \end{Bmatrix} = \begin{bmatrix} D_x & D_1 & 0 \\ D_1 & D_y & 0 \\ 0 & 0 & D_{xy} \end{bmatrix} \begin{Bmatrix} -\frac{\partial^2 w}{\partial x^2} \\ -\frac{\partial^2 w}{\partial y^2} \\ 2\frac{\partial^2 w}{\partial x \partial y} \end{Bmatrix} = \mathbf{D} \cdot \boldsymbol{\varepsilon}, \tag{24}$$

in which the constitutive matrix $\mathbf{D}$ elements is are defined as

$$D_x = \frac{E_x t^3}{12(1-\nu_x \nu_y)}, \quad D_y = \frac{E_y t^3}{12(1-\nu_x \nu_y)}, \quad D_{xy} = \frac{G_{xy} t^3}{12}, \quad D_1 = \nu_x D_y = \nu_y D_x. \tag{25}$$

The total potential energy of the plate consists of the elastic strain energy and the potential energy due to the applied loads. The general form of the potential energy equation can be written as

$$U = \tfrac{1}{2} \int \boldsymbol{\varepsilon}^{\mathrm{T}} \boldsymbol{\sigma} \, \mathrm{d}x \, \mathrm{d}y - \int w(x,y) \, q \, \mathrm{d}x \, \mathrm{d}y \tag{26}$$

By minimizing the potential energy,

$$\mathbf{K} \cdot \boldsymbol{\delta} = \mathbf{F} \tag{27}$$

where $\mathbf{K}$ and $\mathbf{F}$ are the stiffness matrix of the strip and the corresponding load vector of the strip respectively. These two matrices can be stated by utilising equation (23) as

$$\mathbf{K} = \int \mathbf{B}^{\mathrm{T}} \mathbf{D}\, \mathbf{B}\, \mathrm{d}x\, \mathrm{d}y \tag{28}$$

$$\mathbf{F} = \int \left([\mathbf{N}]\, [\boldsymbol{\Psi}] \right)^{\mathrm{T}} q\, \mathrm{d}x\, \mathrm{d}y. \tag{29}$$

4 Enforcement of the essential boundary conditions

The enforcement of boundary conditions in the SFSM is generally attained through the amendment of the local boundary spline function in the longitudinal direction and by adopting the routine finite element approach in the transverse direction. Although the amended splines have been used conventionally for enforcement of the variety of end conditions, these amended splines are fairly difficult to implement, particularly when complex/mixed boundary conditions or internal restraints are present. Vrcelj and Bradford (2008) presented a simple technique for replacing the amendment scheme for imposing boundary conditions. The concept of their technique is based on a full transformation of the nodal coefficients in each strip.

Considering the nodal coefficients vector δ in equation (27), the vector of strip displacement coefficients is defined as

$$\boldsymbol{\delta} = \begin{bmatrix} \mathbf{w}_i & \boldsymbol{\theta}_{iy} & \mathbf{w}_j & \boldsymbol{\theta}_{jy} \end{bmatrix}^{\mathrm{T}}. \tag{30}$$

According to the specifications of the spline function located near the ends of strips, the displacement coefficients contain degrees of freedom which are located outside the strip (additional section knots), e.g. considering the vector $\mathbf{w}_i$, the nodal displacement vector $\bar{\mathbf{w}}_i$ is defined as

$$\bar{\mathbf{w}}_i = \bar{\mathbf{T}}.\mathbf{w}_i, \tag{31}$$

in which $\bar{\mathbf{T}}$ is a transformation matrix and is structured as

$$\bar{\mathbf{T}} = \begin{bmatrix} \frac{-1}{2h} & 0 & \frac{1}{2h} & & & & \\ \frac{1}{6} & \frac{2}{3} & \frac{1}{6} & & & \text{zero} & \\ & \frac{1}{6} & \frac{2}{3} & \frac{1}{6} & & & \\ & & \ldots & \ldots & \ldots & & \\ & & & \frac{1}{6} & \frac{2}{3} & \frac{1}{6} & \\ & \text{zero} & & & \frac{1}{6} & \frac{2}{3} & \frac{1}{6} \\ & & & & \frac{-1}{2h} & 0 & \frac{1}{2h} \end{bmatrix} \tag{32}$$

and

$$\bar{\mathbf{w}}_i = \begin{bmatrix} \bar{w}'_0 & \bar{w}_0 & \bar{w}_1 & \bar{w}_2 & \dots & \bar{w}_{m-1} & \bar{w}_m & \bar{w}'_m \end{bmatrix}_i^{\mathrm{T}}. \tag{33}$$

In fact, in this approach instead of defining the spline coefficients at end and outer knots, i.e. w_{-1}, w_0, w_m, and w_{m+1}, the displacement and rotation at the ends are evaluated. By employing this transformation matrix, the displacement coefficients $\mathbf{w}_i$ are transformed into actual degrees of freedom, and as in the conventional FEM the prescribed boundary conditions can be easily imposed. The same procedure can be performed for other nodal coefficients, and the total transformation matrix for a strip is given concisely by

$$\mathbf{\Lambda} = \left| \bar{\bar{\mathbf{T}}} \;\; \bar{\mathbf{T}} \;\; \bar{\mathbf{T}} \;\; \underline{\bar{\mathbf{T}}} \right|. \tag{34}$$

Having defined the total transformation matrix $\mathbf{\Lambda}$, the transformed stiffness $\bar{\mathbf{K}}$ and the associated load matrix $\bar{\mathbf{F}}$ of the strip can be obtained by relations

$$\bar{\mathbf{K}} = \left(\mathbf{\Lambda}^{-1}\right)^{\mathrm{T}} \mathbf{K} \mathbf{\Lambda}^{-1} \tag{35}$$

$$\bar{\mathbf{F}} = \left(\mathbf{\Lambda}^{-1}\right)^{\mathrm{T}} \mathbf{F}. \tag{36}$$

For the RKP-FSM, the enforcement of the boundary conditions is a little more complex. This complexity is due to the lack of the Kronecker delta property for mesh-free shape functions [Wagner and Liu (2000)]. As a result, several varieties of methods have been proposed in an attempt to enforce the essential boundary conditions as accurately as possible. Amongst these, the most commonly adopted methods are the Lagrange multiplier method, the penalty method, and collocation methods [Chen, Pan, Wu, and Liu (1996)], [Chen and Wang (2000)], [Wagner and Liu (2000)].

Collocation methods for enforcement of the essential boundary conditions are a series of methods in which the boundary conditions are enforced exactly as prescribed at considered particles or nodes. Wagner and Liu (2000) proposed a corrected collocation method for enforcing the essential boundary conditions in kernel-based meshfree methods, such as the conventional RKPM. Although their method was efficient in the context of the RKPM, it could not be applied in the generalised RKPM since it was not suited for the enforcement of derivative-type boundary conditions. In response, Behzadan, Shodja, and Khezri (2011) developed the corrected collocation method further, and proposed the generalised collocation method, which was a suitable tool for enforcement of any kind of boundary conditions in the context of the generalised RKPM. Herein, since the generalised RKPM has been used as the approximation tool in the longitudinal direction of the strips, the same generalised collocation method is applicable. This method was described in detail by Behzadan, Shodja, and Khezri (2011), and for brevity is not presented here.

5 Treatment of material discontinuities

Techniques for the modelling of abrupt changes in the plate thickness and step changes of material properties in an efficient and accurate manner by utilising the SFSM have received significant attention. The most common approach in dealing with these appears to be the application of the general spline finite strip method (G-s FSM) [Dawe and Tan (2002)]. An important consideration in the bending analysis of plates with abrupt thickness changes or step changes in material properties is the order of continuity of the considered displacement field, i.e. at a step change of the material properties the deflection w and its derivatives must be continuous, while the curvatures have to be discontinuous. Therefore, the requirement is a displacement field with C^1 continuity, but the conventional SFSM approximated field has C^2 continuity. To circumvent this deficiency, Dawe and Tan (2002) have adopted the G-s FSM and used the method's flexibility in spacing knots to reduce the continuity order at break points by moving two or more knots together such that they coincide at the breakpoint. However in their study, due to some practical reasons associated with the use of super-strips, a different approach has been preceded and a compact configuration of section knots has been used in the vicinity of the influencing area. Although this approach is acceptable for calculation of natural frequencies and buckling loads, for a static analysis of plates such as a bending analysis, the procedure may encounter numerical problems and possible fluctuations in the results, especially in the stress distribution. It is noteworthy that the condition of accuracy of the results obtained may deteriorate when the ratio of the stiffness properties of the plate segments increases. In the rest of this section, a straightforward methodology for inclusion of abrupt stiffness changes in the longitudinal direction of plates in the SFSM is presented.

Shodja, Khezri, Hashemian, and Behzadan (2010) added new capabilities to the generalised RKPM by extending the corrected collocation method for the numerical analysis of multi-phase domains. In their study, the augmented collocation method was applied successfully for the determination of elastic fields of multi-phase medias, particularly problems of circular inhomogeneous inclusion, and the interaction of cracks with embedded inhomogeneity. Herein, since the generalised RKPM shape functions are used in the longitudinal-direction approximation of the proposed RKP-FSM, the augmented collocation method is used for the treatment of material discontinuities.

For the treatment of material discontinuities in the conventional SFSM, a similar concept of the augmented collocation method, but with the required modification for the SFSM formulation, is developed here. Consider a rectangular plate with a form of material discontinuity in its longitudinal direction (Fig. 4). To begin, assume that a fictitious line $\mathbf{\Gamma}_{AB}$ is placed along the break line of the material prop-

erties or the line of abrupt change in thickness. This line divides the plate domain into two separate parts, viz. A and B. Henceforth, this line will be referred to as the interface boundary.

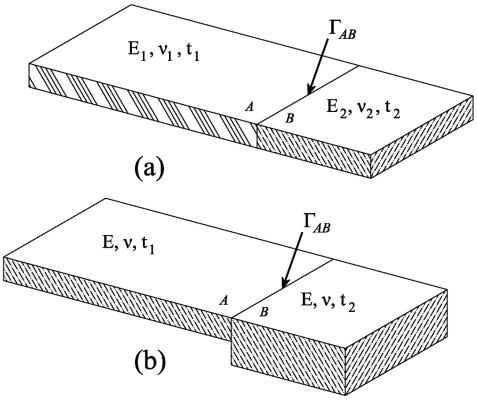

Figure 4: Rectangular plates with forms of material and thickness discontinuity

Each of the considered domains A and B are considered as separate phases and are discretised individually using the same number of strips (n) for both phases while the number of segments in each phase is independent from the other phase. Accordingly, the matrix representation of the weak form of the plate-bending differential equation for these phases can be stated separately as

$$\begin{cases} \bar{\mathbf{c}}^{A\,\mathrm{T}} \cdot \left(\bar{\mathbf{K}}\mathbf{t}^{A} \mathbf{d}^{A} - \bar{\mathbf{F}}\mathbf{t}^{A} \right) = 0 \\ \bar{\mathbf{c}}^{B\,\mathrm{T}} \cdot \left(\bar{\mathbf{K}}\mathbf{t}^{B} \mathbf{d}^{B} - \bar{\mathbf{F}}\mathbf{t}^{B} \right) = 0 \end{cases}, \tag{37}$$

in which $\bar{\mathbf{K}}\mathbf{t}^{\alpha}$, and $\bar{\mathbf{F}}\mathbf{t}^{\alpha}$ $(\alpha = A, B)$ are the global stiffness matrix and load vector of each phase which are assembled using the transformed strip stiffnesses and load vectors (equations (35) and (36)), and $\bar{\mathbf{c}}^{\alpha}$ $(\alpha = A, B)$ are column vectors of arbitrary coefficients. In addition, $\mathbf{d}^{\alpha}(\alpha = A, B)$ are the total displacements vectors of the phases, defined as

$$\bar{\mathbf{d}}^{\alpha} = \left[\boldsymbol{\delta}_1^{\alpha} \quad \boldsymbol{\delta}_2^{\alpha} \quad \ldots \quad \boldsymbol{\delta}_{n+1}^{\alpha} \right]^{\mathrm{T}} \qquad \alpha = A, B. \tag{38}$$

Equations (37) may be written alternatively using matrix notation as

$$\left[\bar{\mathbf{c}}^{A\mathrm{T}} \quad \bar{\mathbf{c}}^{B\mathrm{T}} \right] \left(\begin{bmatrix} \bar{\mathbf{K}}\mathbf{t}^{A} & \\ & \bar{\mathbf{K}}\mathbf{t}^{B} \end{bmatrix} \begin{bmatrix} \bar{\mathbf{d}}^{A} \\ \bar{\mathbf{d}}^{B} \end{bmatrix} - \begin{bmatrix} \bar{\mathbf{f}}\mathbf{t}^{A} \\ \bar{\mathbf{f}}\mathbf{t}^{B} \end{bmatrix} \right) = 0. \tag{39}$$

The degrees of freedom in each phase are numbered using the scheme described below:

1. The first category are DOFs in which the essential boundary conditions are defined and denoted using a subscript e.

2. The second group are DOFs located along the interface line. Since the same number of strips has been used in both phases, number of DOFs are the same for both phases. A subscript i will be used to denote the related variables.

3. Finally, the remaining DOFs are denoted using r as the subscript.

For instance, using this numbering pattern, the displacements vectors of phases defined in equation (38) can be rewritten as

$$\bar{\mathbf{d}}^{\alpha} = \begin{bmatrix} \bar{\mathbf{d}}_e^{\alpha} & \bar{\mathbf{d}}_i^{\alpha} & \bar{\mathbf{d}}_r^{\alpha} \end{bmatrix}^{\mathrm{T}} \qquad \alpha = A, B. \tag{40}$$

In the same manner, using the numbering scheme the matrices in relation (39) can be partitioned and presented as

$$\begin{bmatrix} \bar{\mathbf{c}}_e^{A\mathrm{T}} \\ \bar{\mathbf{c}}_i^{A\mathrm{T}} \\ \bar{\mathbf{c}}_r^{A\mathrm{T}} \\ \bar{\mathbf{c}}_e^{B\mathrm{T}} \\ \bar{\mathbf{c}}_i^{B\mathrm{T}} \\ \bar{\mathbf{c}}_r^{B\mathrm{T}} \end{bmatrix}^{T} \left(\begin{bmatrix} \bar{\mathbf{K}}\mathbf{t}_{ee}^{A} & \bar{\mathbf{K}}\mathbf{t}_{ei}^{A} & \bar{\mathbf{K}}\mathbf{t}_{er}^{A} & 0 & 0 & 0 \\ \bar{\mathbf{K}}\mathbf{t}_{ie}^{A} & \bar{\mathbf{K}}\mathbf{t}_{ii}^{A} & \bar{\mathbf{K}}\mathbf{t}_{ir}^{A} & 0 & 0 & 0 \\ \bar{\mathbf{K}}\mathbf{t}_{re}^{A} & \bar{\mathbf{K}}\mathbf{t}_{ri}^{A} & \bar{\mathbf{K}}\mathbf{t}_{rr}^{A} & 0 & 0 & 0 \\ 0 & 0 & 0 & \bar{\mathbf{K}}\mathbf{t}_{ee}^{B} & \bar{\mathbf{K}}\mathbf{t}_{ei}^{B} & \bar{\mathbf{K}}\mathbf{t}_{er}^{B} \\ 0 & 0 & 0 & \bar{\mathbf{K}}\mathbf{t}_{ie}^{B} & \bar{\mathbf{K}}\mathbf{t}_{ii}^{B} & \bar{\mathbf{K}}\mathbf{t}_{ir}^{B} \\ 0 & 0 & 0 & \bar{\mathbf{K}}\mathbf{t}_{re}^{B} & \bar{\mathbf{K}}\mathbf{t}_{ri}^{B} & \bar{\mathbf{K}}\mathbf{t}_{rr}^{B} \end{bmatrix} \begin{bmatrix} \bar{\mathbf{d}}_e^{A} \\ \bar{\mathbf{d}}_i^{A} \\ \bar{\mathbf{d}}_r^{A} \\ \bar{\mathbf{d}}_e^{B} \\ \bar{\mathbf{d}}_i^{B} \\ \bar{\mathbf{d}}_r^{B} \end{bmatrix} - \begin{bmatrix} \bar{\mathbf{f}}\mathbf{t}_e^{A} \\ \bar{\mathbf{f}}\mathbf{t}_i^{A} \\ \bar{\mathbf{f}}\mathbf{t}_r^{A} \\ \bar{\mathbf{f}}\mathbf{t}_e^{B} \\ \bar{\mathbf{f}}\mathbf{t}_i^{B} \\ \bar{\mathbf{f}}\mathbf{t}_r^{B} \end{bmatrix} \right) = \{0\}. \tag{41}$$

In the next step, all of the DOFs in both phases are numbered again using the same numbering pattern which was used for numbering each phase. It should be noted that in this step, numbering is performed such that those DOFs which are located on the interface boundary and correspond to the same component of the displacement or rotation (one in phase A, and the other in phase B) are placed in sequential order. Employing the global partitioning order, equation (41) takes the form

$$\begin{bmatrix} \bar{\mathbf{c}}_e^{A\mathrm{T}} \\ \bar{\mathbf{c}}_e^{B\mathrm{T}} \\ \bar{\mathbf{c}}_i^{A\mathrm{T}} \\ \bar{\mathbf{c}}_i^{B\mathrm{T}} \\ \bar{\mathbf{c}}_r^{A\mathrm{T}} \\ \bar{\mathbf{c}}_r^{B\mathrm{T}} \end{bmatrix}^{T} \left(\begin{bmatrix} \bar{\mathbf{K}}\mathbf{t}_{ee}^{A} & 0 & \bar{\mathbf{K}}\mathbf{t}_{ei}^{A} & 0 & \bar{\mathbf{K}}\mathbf{t}_{er}^{A} & 0 \\ 0 & \bar{\mathbf{K}}\mathbf{t}_{ee}^{B} & 0 & \bar{\mathbf{K}}\mathbf{t}_{ei}^{B} & 0 & \bar{\mathbf{K}}\mathbf{t}_{er}^{B} \\ \bar{\mathbf{K}}\mathbf{t}_{ie}^{A} & 0 & \bar{\mathbf{K}}\mathbf{t}_{ii}^{A} & 0 & \bar{\mathbf{K}}\mathbf{t}_{ir}^{A} & 0 \\ 0 & \bar{\mathbf{K}}\mathbf{t}_{ie}^{B} & 0 & \bar{\mathbf{K}}\mathbf{t}_{ii}^{B} & 0 & \bar{\mathbf{K}}\mathbf{t}_{ir}^{B} \\ \bar{\mathbf{K}}\mathbf{t}_{re}^{A} & 0 & \bar{\mathbf{K}}\mathbf{t}_{ri}^{A} & 0 & \bar{\mathbf{K}}\mathbf{t}_{rr}^{A} & 0 \\ 0 & \bar{\mathbf{K}}\mathbf{t}_{re}^{B} & 0 & \bar{\mathbf{K}}\mathbf{t}_{ri}^{B} & 0 & \bar{\mathbf{K}}\mathbf{t}_{rr}^{B} \end{bmatrix} \begin{bmatrix} \bar{\mathbf{d}}_e^{A} \\ \bar{\mathbf{d}}_e^{B} \\ \bar{\mathbf{d}}_i^{A} \\ \bar{\mathbf{d}}_i^{B} \\ \bar{\mathbf{d}}_r^{A} \\ \bar{\mathbf{d}}_r^{B} \end{bmatrix} - \begin{bmatrix} \bar{\mathbf{f}}\mathbf{t}_e^{A} \\ \bar{\mathbf{f}}\mathbf{t}_e^{B} \\ \bar{\mathbf{f}}\mathbf{t}_i^{A} \\ \bar{\mathbf{f}}\mathbf{t}_i^{B} \\ \bar{\mathbf{f}}\mathbf{t}_r^{A} \\ \bar{\mathbf{f}}\mathbf{t}_r^{B} \end{bmatrix} \right) = \{0\}. \tag{42}$$

Defining the vector $\mathbf{R}$ as

$$\mathbf{R}=\begin{bmatrix}\bar{\mathbf{r}}_e^{A\mathrm{T}}\\ \bar{\mathbf{r}}_e^{B\mathrm{T}}\\ \bar{\mathbf{r}}_i^{A\mathrm{T}}\\ \bar{\mathbf{r}}_i^{B\mathrm{T}}\\ \bar{\mathbf{r}}_r^{A\mathrm{T}}\\ \bar{\mathbf{r}}_r^{B\mathrm{T}}\end{bmatrix}=\left(\begin{bmatrix}\bar{\mathbf{K}}\mathbf{t}_{ee}^{A} & 0 & \bar{\mathbf{K}}\mathbf{t}_{ei}^{A} & 0 & \bar{\mathbf{K}}\mathbf{t}_{er}^{A} & 0\\ 0 & \bar{\mathbf{K}}\mathbf{t}_{ee}^{B} & 0 & \bar{\mathbf{K}}\mathbf{t}_{ei}^{B} & 0 & \bar{\mathbf{K}}\mathbf{t}_{er}^{B}\\ \bar{\mathbf{K}}\mathbf{t}_{ie}^{A} & 0 & \bar{\mathbf{K}}\mathbf{t}_{ii}^{A} & 0 & \bar{\mathbf{K}}\mathbf{t}_{ir}^{A} & 0\\ 0 & \bar{\mathbf{K}}\mathbf{t}_{ie}^{B} & 0 & \bar{\mathbf{K}}\mathbf{t}_{ii}^{B} & 0 & \bar{\mathbf{K}}\mathbf{t}_{ir}^{B}\\ \bar{\mathbf{K}}\mathbf{t}_{re}^{A} & 0 & \bar{\mathbf{K}}\mathbf{t}_{ri}^{A} & 0 & \bar{\mathbf{K}}\mathbf{t}_{rr}^{A} & 0\\ 0 & \bar{\mathbf{K}}\mathbf{t}_{re}^{B} & 0 & \bar{\mathbf{K}}\mathbf{t}_{ri}^{B} & 0 & \bar{\mathbf{K}}\mathbf{t}_{rr}^{B}\end{bmatrix}\begin{bmatrix}\bar{\mathbf{d}}_e^{A}\\ \bar{\mathbf{d}}_e^{B}\\ \bar{\mathbf{d}}_i^{A}\\ \bar{\mathbf{d}}_i^{B}\\ \bar{\mathbf{d}}_r^{A}\\ \bar{\mathbf{d}}_r^{B}\end{bmatrix}-\begin{bmatrix}\bar{\mathbf{f}}\mathbf{t}_e^{A}\\ \bar{\mathbf{f}}\mathbf{t}_e^{B}\\ \bar{\mathbf{f}}\mathbf{t}_i^{A}\\ \bar{\mathbf{f}}\mathbf{t}_i^{B}\\ \bar{\mathbf{f}}\mathbf{t}_r^{A}\\ \bar{\mathbf{f}}\mathbf{t}_r^{B}\end{bmatrix}\right),\tag{43}$$

the relation (42) can be reformed as

$$\bar{\mathbf{c}}_e^{A\mathrm{T}}\bar{\mathbf{c}}_e^{A}+\bar{\mathbf{c}}_e^{B\mathrm{T}}\bar{\mathbf{r}}_e^{B}+\bar{\mathbf{c}}_i^{A\mathrm{T}}\bar{\mathbf{r}}_i^{A}+\bar{\mathbf{c}}_i^{B\mathrm{T}}\bar{\mathbf{r}}_i^{B}+\bar{\mathbf{c}}_r^{A\mathrm{T}}\bar{\mathbf{r}}_r^{A}+\bar{\mathbf{c}}_r^{B\mathrm{T}}\bar{\mathbf{r}}_r^{B}=0.\tag{44}$$

Note that the coefficients $\bar{\mathbf{c}}_e^{A}$, and $\bar{\mathbf{c}}_e^{B}$ are associated with essential boundary conditions and, therefore

$$\bar{\mathbf{c}}_e^{A}=\bar{\mathbf{c}}_e^{B}=0.\tag{45}$$

Also, since $\bar{\mathbf{c}}_i^{A}$, and $\bar{\mathbf{c}}_i^{B}$ are associated with DOFs which are located on the interface boundary and basically are the same nodal value, it can be assumed that

$$\bar{\mathbf{c}}_i^{A}=\bar{\mathbf{c}}_i^{B}=\text{Arbitrary}\tag{46}$$

and finally for the remaining degrees of freedom

$$\bar{\mathbf{c}}_r^{A},\bar{\mathbf{c}}_r^{B}=\text{Arbitrary}.\tag{47}$$

Substituting relations (45)-(47) in equation (44) results in

$$\begin{aligned}&\bar{\mathbf{c}}_i^{A\mathrm{T}}\left(\bar{\mathbf{r}}_i^{A}+\bar{\mathbf{r}}_i^{B}\right)+\bar{\mathbf{c}}_r^{A\mathrm{T}}\bar{\mathbf{r}}_r^{A}+\bar{\mathbf{c}}_r^{B\mathrm{T}}\bar{\mathbf{r}}_r^{B}=0\\ &\bar{\mathbf{c}}_i^{A},\ \bar{\mathbf{c}}_r^{A},\ \bar{\mathbf{c}}_r^{B}=\text{Arbitrary}.\end{aligned}\tag{48}$$

Hence, from equation (48), it can be concluded directly that

$$\begin{cases}\bar{\mathbf{r}}_i^{A}+\bar{\mathbf{r}}_i^{B}=0\\ \bar{\mathbf{r}}_r^{A}=0\\ \bar{\mathbf{r}}_r^{B}=0.\end{cases}\tag{49}$$

Considering equations (43), and (49), the equation

$$\begin{bmatrix}\bar{\mathbf{K}}\mathbf{t}_{ie}^{A} & \bar{\mathbf{K}}\mathbf{t}_{ie}^{B} & \bar{\mathbf{K}}\mathbf{t}_{ii}^{A} & \bar{\mathbf{K}}\mathbf{t}_{ii}^{B} & \bar{\mathbf{K}}\mathbf{t}_{ir}^{A} & \bar{\mathbf{K}}\mathbf{t}_{ir}^{B}\\ \bar{\mathbf{K}}\mathbf{t}_{re}^{A} & 0 & \bar{\mathbf{K}}\mathbf{t}_{ri}^{A} & 0 & \bar{\mathbf{K}}\mathbf{t}_{rr}^{A} & 0\\ 0 & \bar{\mathbf{K}}\mathbf{t}_{re}^{B} & 0 & \bar{\mathbf{K}}\mathbf{t}_{ri}^{B} & 0 & \bar{\mathbf{K}}\mathbf{t}_{rr}^{B}\end{bmatrix}\begin{bmatrix}\bar{\mathbf{d}}_e^{A}\\ \bar{\mathbf{d}}_e^{B}\\ \bar{\mathbf{d}}_i^{A}\\ \bar{\mathbf{d}}_i^{B}\\ \bar{\mathbf{d}}_r^{A}\\ \bar{\mathbf{d}}_r^{B}\end{bmatrix}=\begin{bmatrix}\bar{\mathbf{f}}\mathbf{t}_i^{A}+\bar{\mathbf{f}}\mathbf{t}_i^{B}\\ \bar{\mathbf{f}}\mathbf{t}_r^{A}\\ \bar{\mathbf{f}}\mathbf{t}_r^{B}\end{bmatrix}\tag{50}$$

can be derived. It should be noted that $\bar{\mathbf{d}}_e^A$, and $\bar{\mathbf{d}}_e^B$ are nodal values associated with the essential boundary conditions and their values are known, and also it is evident that $\bar{\mathbf{d}}_i^A$, and $\bar{\mathbf{d}}_i^B$ are associated with the same nodal displacements $\bar{\mathbf{d}}_i^A = \bar{\mathbf{d}}_i^B$. Thus, the equation (50) takes the form

$$\begin{bmatrix} \bar{\mathbf{K}}\mathbf{t}_{ii}^A + \bar{\mathbf{K}}\mathbf{t}_{ii}^B & \bar{\mathbf{K}}\mathbf{t}_{ir}^A & \bar{\mathbf{K}}\mathbf{t}_{ir}^B \\ \bar{\mathbf{K}}\mathbf{t}_{ri}^A & \bar{\mathbf{K}}\mathbf{t}_{rr}^A & 0 \\ \bar{\mathbf{K}}\mathbf{t}_{ri}^B & 0 & \bar{\mathbf{K}}\mathbf{t}_{rr}^B \end{bmatrix} \begin{bmatrix} \bar{\mathbf{d}}_i^A \\ \bar{\mathbf{d}}_r^A \\ \bar{\mathbf{d}}_r^B \end{bmatrix} = \begin{bmatrix} \bar{\mathbf{f}}\mathbf{t}_i^A + \bar{\mathbf{f}}\mathbf{t}_i^B \\ \bar{\mathbf{f}}\mathbf{t}_r^A \\ \bar{\mathbf{f}}\mathbf{t}_r^B \end{bmatrix} - \begin{bmatrix} \bar{\mathbf{K}}\mathbf{t}_{ie}^A & \bar{\mathbf{K}}\mathbf{t}_{ie}^B \\ \bar{\mathbf{K}}\mathbf{t}_{re}^A & 0 \\ 0 & \bar{\mathbf{K}}\mathbf{t}_{re}^B \end{bmatrix} \begin{bmatrix} \bar{\mathbf{d}}_e^A \\ \bar{\mathbf{d}}_e^B \end{bmatrix}. \tag{51}$$

By solving equation (51), all unknown nodal values can be determined.

6 Numerical results

A number of problems are solved here to demonstrate the efficiency, versatility, robustness and accuracy of the proposed methodologies. These problems consider rectangular plates having length dimensions a and b in the x and y directions respectively, with the Cartesian coordinate origin at the centre of the plate. To classify the plate bending problems according to the support condition on each edge, a notation has been adopted such that, for example, the nomenclature $C-S-F-S$ indicates a rectangular plate whose edges $x=-a/2$ and $x=+a/2$ are simply supported, and edges $y=-b/2$ and $y=+b/2$ are clamped and free respectively.

6.1 Square plates with two opposite edges simply-supported and with arbitrary support conditions on the other two opposite edges

In this example, to examine the performance of the generalised RKP-FSM, square thin plates with two opposite edges simply supported and arbitrary support conditions on the remaining edges and subjected to uniform loads are analysed, and the convergence and numerical accuracy are studied. Fig. 5 shows the plates studied and possible symmetries are utilised.

These support configurations are selected because the exact solutions for these problems were proposed by Levy (1899). The exact solutions in form of an infinite Fourier series can be found in the paper of Ventsel, and Krauthammer (2001).

In each configuration the plate is discretised using *NS* equal strips and every strip is divided into *NP* equal parts. The parameter h, which represents the average mesh size, is defined as $(a/NS+b/NP)/2$, where a and b denote the plate dimensions in the x and y directions. The first example is solved by the generalised RKP-FSM and SFSM, and the convergence rate of the methods in L^2, H^1 and H^2norms are presented in Fig. 6 for each case in a separate error diagram. The corresponding diagrams have been obtained using the 4×6, 6×9, 8×12, 10×15, 12×18 and

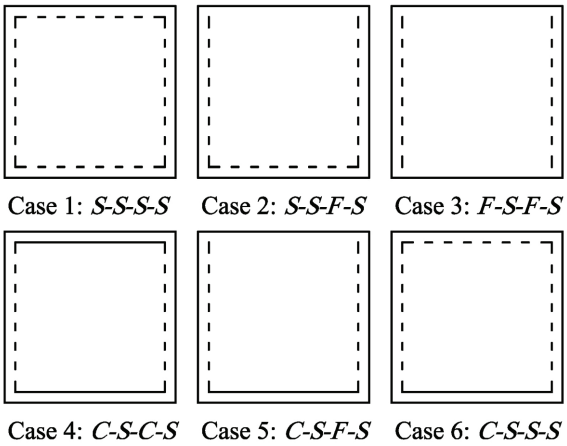

Figure 5: Six plate support configurations (S = simply supported; C = clamped; F = free)

14×21 patterns for stripping and segmenting of plates. Fig. 7 shows the numerical results obtained from the RKP-SFM.

6.2 Square plates subjected to uniform load using non-uniform meshes

As was stated previously, one of the attractive features of the new method is that it allows for the arbitrary placement of nodes in the longitudinal direction, which enriches the method with a versatile and powerful capability for the solution of problems with steep gradients, intermediate supports, and the like. This feature allows for the local refinement of the mesh in the vicinity of the areas in which a denser mesh configuration is required for obtaining more accurate results. To this end, this example is designed to examine the performance of the generalised RKP-FSM in solving thin-plate bending problems using unequally spaced meshes. A similar example, but with a different configuration and discretisation scheme, was used by Gutkowski, Chen, and Puckett (1991) for the evaluation of the SFSM with unequally spaced splines.

Three symmetric configurations of the support conditions for a square plate subjected to uniform load are assumed as$S-S-S-S$, $F-S-F-S$, $C-S-C-S$. Analyses for each case were performed using 6×8, 8×12, 12×18, and 16×24 mesh patterns, in which the first number indicates the number of strips used in the analysis and the second number is the number of segments in the longitudinal direction. In order to verify the accuracy and convergence of the proposed method using non-uniform meshes, two distinct mesh categories are adopted. In the first, which will

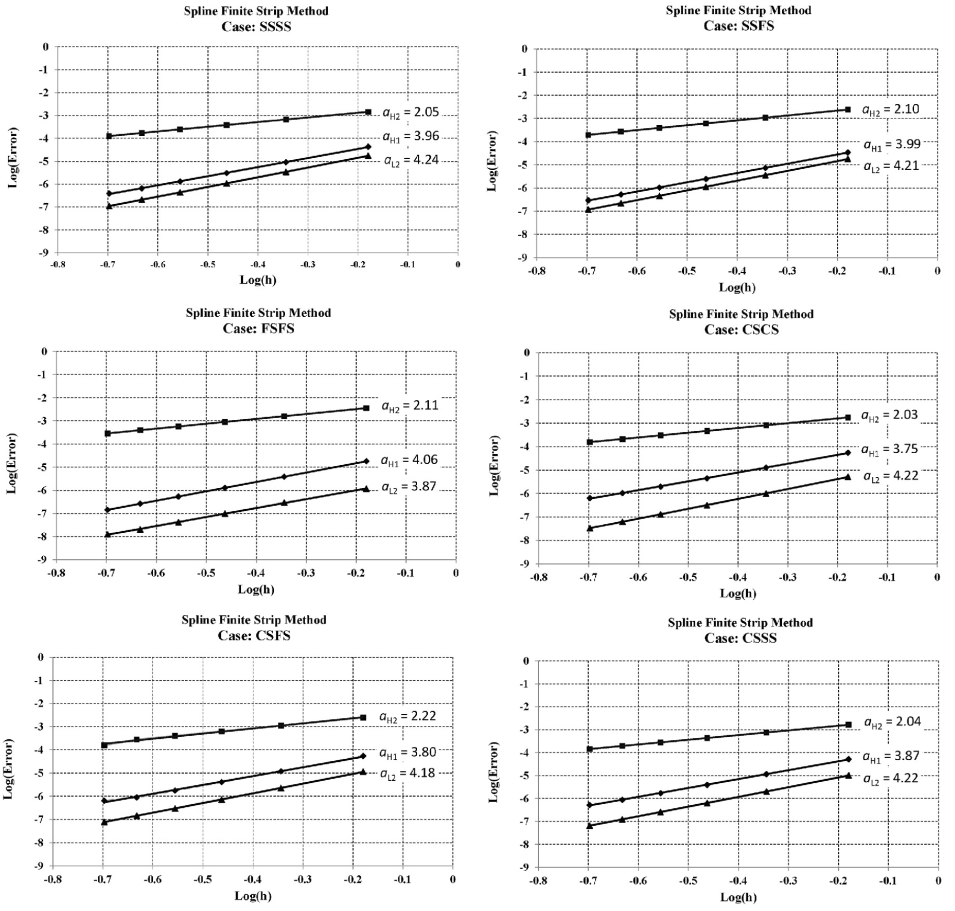

Figure 6: Errors in L^2, H^1, and H^2 norms using SFSM for various configurations

be referred to as an equally-spaced mesh, the strips and sections are placed uniformly while in the second category, which will referred to as an unequally-spaced mesh, the refinement patterns have been adopted to ensure the construction of a finer mesh in the centre area of the plates. These discretisation configurations are shown in Fig. 8.

The results obtained for the dimensionless central moment in the x direction M_x using a non-uniform mesh are tabulated for each case in Tables 1 to 3, and are compared with equally spaced meshes.

The results presented demonstrate excellent accuracy and improved convergence for the central moments for unequally spaced meshes. It is apparent that the errors

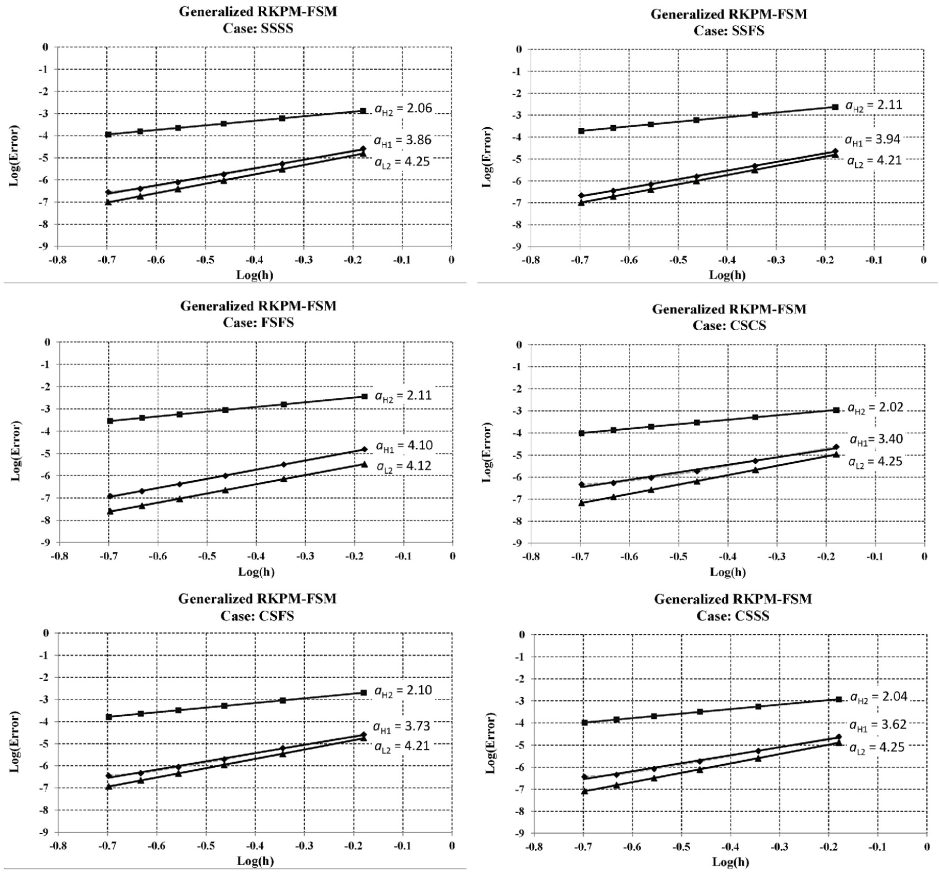

Figure 7: Errors in L^2, H^1, and H^2 norms using Generalised RKP-FSM for various configurations

decrease by utilising the feature of the method for mesh refinement.

6.3 Analysis of rectangular plate simply supported on all edges subjected to a patch load

A thin rectangular plate is taken to be simply supported on all edges and supporting a constant patch load of intensity q is shown in Fig. 9. A similar example has been used by Burgess, and Mahajerin (1985) to verify a numerical method for laterally loaded thin plates. A classical solution for this problem by infinite double trigonometric series was given by Szilard (2004), and by Ventsel, and Krauthammer (2001).

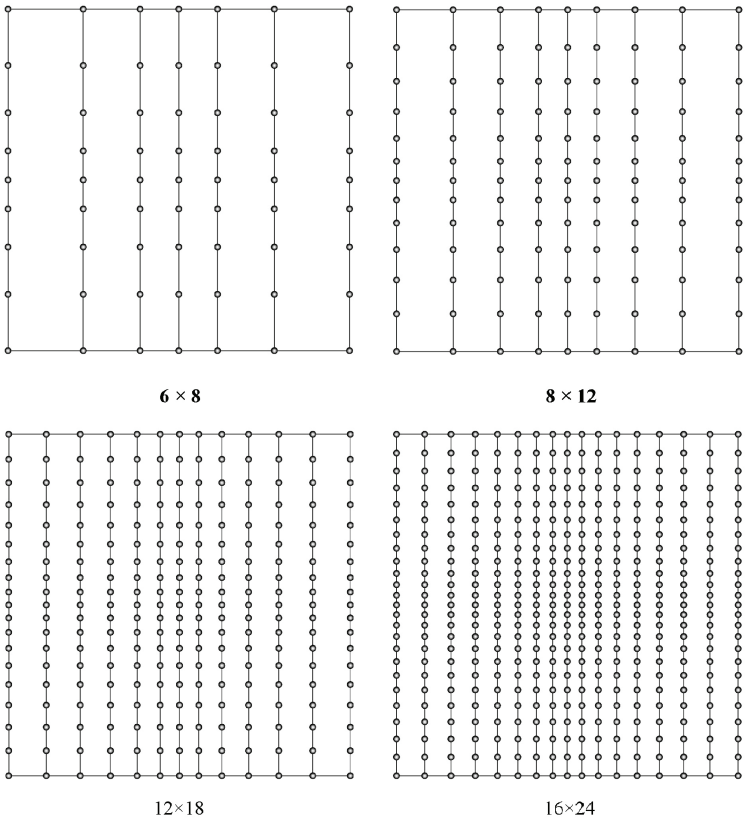

Figure 8: Unequally spaced meshes

Table 1: Central moment for $S-S-S-S$ plate under uniform load

Generalized RKPM-FSM

Strips × Sections	C_1		% of error	
	Equally Spaced	*Unequally spaced*	*Equally Spaced*	*Unequally spaced*
6 × 8	0.04831	0.04805	0.860	0.319
8 × 12	0.04811	0.04800	0.441	0.212
12 × 18	0.04798	0.04793	0.169	0.073
16 × 24	0.04794	0.04791	0.089	0.032

M_x - Classical solution: 0.04789 Centre moment: $C_1 \times q \times L^2$

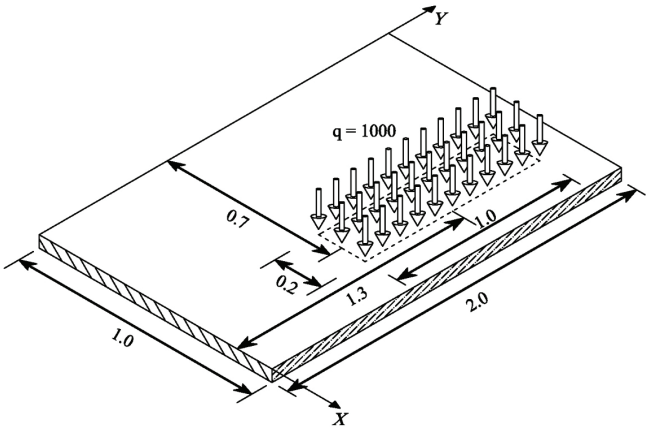

Figure 9: Rectangular simply supported plate subjected to a patch load

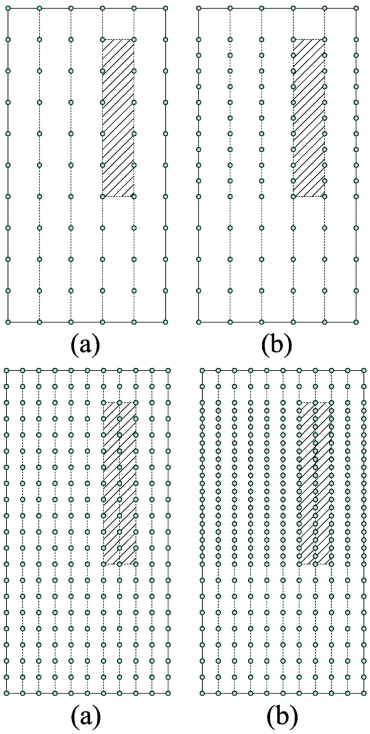

Figure 10: Meshes: (a) uniform; (b) refined using extra knots

Table 2: Central moment for $F-S-F-S$ plate under uniform load

Generalized RKPM-FSM

Strips × Sections	C_2		% of error	
	Equally Spaced	*Unequally spaced*	*Equally Spaced*	*Unequally spaced*
6 × 8	0.124898	0.123620	1.913	0.870
8 × 12	0.123866	0.123164	1.071	0.498
12 × 18	0.123130	0.122960	0.470	0.332
16 × 24	0.122875	0.122698	0.262	0.118

M_x - Classical solution: 0.122553 Centre moment: $C_2 \times q \times L^2$

Table 3: Central moment for $C-S-C-S$ plate under uniform load

Generalized RKPM-FSM

Strips × Section	C_3		% of error	
	Equally Spaced	*Unequally spaced*	*Equally Spaced*	*Unequally spaced*
6 × 8	0.024113	0.024259	1.159	0.559
8 × 12	0.024253	0.024341	0.585	0.224
12 × 16	0.024325	0.024373	0.290	0.091
16 × 24	0.024350	0.024380	0.185	0.065

M_x - Classical solution: 0.024396 Centre moment: $C_3 \times q \times L^2$

This example examines the effect of local refinement of the nodes in the longitudinal direction of the nodal lines in the vicinity of interest in influencing effects such as patch loads. To this end, two uniform discretisation schemes are adopted using 5×10 and 10×20 strips and segments. In order to study the effects of refinement, two new refined meshes are generated with only a minor change by adding extra knots on each nodal line in the area that is supporting the assumed patch load. These two discretisation patterns are depicted in Fig. 10. To verify the improvements in the results obtained for the vertical displacement of the plate, 12 nodes surrounding the patch load are chosen and the numerical results obtained using RKP-FSM are compared with the exact solutions.

For comparison, the results for the deflections are evaluated in the representing nodes using the proposed numerical technique and are tabulated in Tables 4 and 5 for the uniform and refined meshes, and are compared with the exact values.

Table 4: Deflection results and error percentage for problem 3 using 5×10 mesh and refined mesh

Results using first discretization scheme:

(x, y)	***Classical Sol.***	***Uniform mesh***	% of error $\times 10^{-2}$	***Refined Mesh***	% of error $\times 10^{-2}$
(0.6, 0.8)	-0.057257146	-0.057255519	0.2841	-0.057257305	0.0277
(0.6, 1.0)	-0.072535371	-0.072542944	1.0440	-0.072535450	0.0108
(0.6, 1.2)	-0.079044095	-0.079045379	0.1625	-0.079044052	0.0054
(0.6, 1.4)	-0.074873440	-0.074871583	0.2480	-0.074873455	0.0019
(0.6, 1.6)	-0.059265549	-0.059267207	0.2797	-0.059265551	0.0003
(0.6, 1.8)	-0.032682654	-0.032679332	1.0164	-0.032682666	0.0038
(0.8, 0.8)	-0.038405346	-0.038403852	0.3890	-0.038405519	0.0450
(0.8, 1.0)	-0.049451483	-0.049459019	1.5241	-0.049451552	0.0141
(0.8, 1.2)	-0.054185671	-0.054186857	0.2190	-0.054185626	0.0083
(0.8, 1.4)	-0.051564159	-0.051562214	0.3771	-0.051564187	0.0056
(0.8, 1.6)	-0.041065512	-0.041067080	0.3818	-0.041065506	0.0016
(0.8, 1.8)	-0.022684357	-0.022681059	1.4537	-0.022684373	0.0069

Table 5: Deflection results and error percentage for problem 3 using 10×20 mesh and refined mesh

Results using second discretization scheme:

(x, y)	***Classical Sol.***	***Uniform mesh***	% of error $\times 10^{-4}$	***Refined Mesh***	% of error $\times 10^{-4}$
(0.6, 0.8)	-0.057257146	-0.057257155	0.1651	-0.057257146	0.0042
(0.6, 1.0)	-0.072535371	-0.072535413	0.5806	-0.072535366	0.0761
(0.6, 1.2)	-0.079044095	-0.079044049	0.5757	-0.079044097	0.0362
(0.6, 1.4)	-0.074873440	-0.074873436	0.0587	-0.074873439	0.0208
(0.6, 1.6)	-0.059265549	-0.059265605	0.9449	-0.059265551	0.0257
(0.6, 1.8)	-0.032682654	-0.032682636	0.5442	-0.032682653	0.0307
(0.8, 0.8)	-0.038405346	-0.038405358	0.3246	-0.038405346	0.0099
(0.8, 1.0)	-0.049451483	-0.049451515	0.6606	-0.049451477	0.1117
(0.8, 1.2)	-0.054185671	-0.054185622	0.9092	-0.054185674	0.0573
(0.8, 1.4)	-0.051564159	-0.051564149	0.1817	-0.051564158	0.0140
(0.8, 1.6)	-0.041065512	-0.041065552	0.9810	-0.041065514	0.0464
(0.8, 1.8)	-0.022684357	-0.022684337	0.8779	-0.022684356	0.0326

It can be concluded from the results presented that the errors obtained for the representative points in the boundary of the patch have been dramatically decreased utilising a refinement pattern in the vicinity of the patch load. This is because the additional nodes improve the efficiency of the method in capturing the field condition in the supporting region of the patch load. The influencing local changes such as patch loads and mid-span supports are among the key justifying reasons for the application of the new RKP-FSM, since unequal spacing and local refinement of the mesh can be performed easily in such problems.

6.4 Analysis of bi-material rectangular plate subjected to a uniform load

In this example, the bending of bi-material thin plates with various boundary conditions is analysed using the SFSM and RKP-FSM, and the accuracy of these methods is demonstrated by a comparison with results obtained using ABAQUS. The material discontinuity between the phases in the plate has been treated via the developed collocation method for the SFSM and the augmented corrected collocation method for the RKP-FSM [Shodja, Khezri, Hashemian, and Behzadan (2010)].

The rectangular plate has two distinctive material phases with the dimensions $a = 5$, $b = 10$ and $t = 0.3$ units, and subjected to a uniformly distributed load of $q = 1$ unit. The material-interface boundary divides the plate into two square 5×5 regions with different material properties. An imaginary data sampling line AB is positioned in the longitudinal direction of the plate passing both phases (Fig. 11). The results obtained for the deflection (w) and component of stress (S_{XX}) along this line have been compared with results obtained form ABAQUS for the same model. It is noteworthy that although in the example only the case of bi-material plates has been examined, the same procedure and treatment method can be applied for plates with abrupt changes in their thickness. The reason is that the changes in the thickness or material properties both results in changes in property matrix D, so the same augmented collocation method is applicable.

For numerical modelling purposes each material phase is discretised separately using 20×20 strips and segments respectively (Fig. 12). The same problem has been modelled using ABAQUS using a very fine mesh constructed by 50×100 elements in order to obtain more accurate results. The same sampling line has been used to collect data in the ABAQUS model.

The three cases $S-F-S-F$, $C-F-C-F$ and $C-F-F-F$ have been analysed and in order to emphasise the performance of the augmented collocation method, no constraint has been imposed on the longitudinal edges and these boundaries have been left free. The elastic modulus for the phase 1 in the first two cases has been taken as 2.1×10^6, while in the third case to prevent large and possible plastic deformations it is taken as 2.1×10^7. In all cases, Poisson's ratio equals $\nu = 0.3$

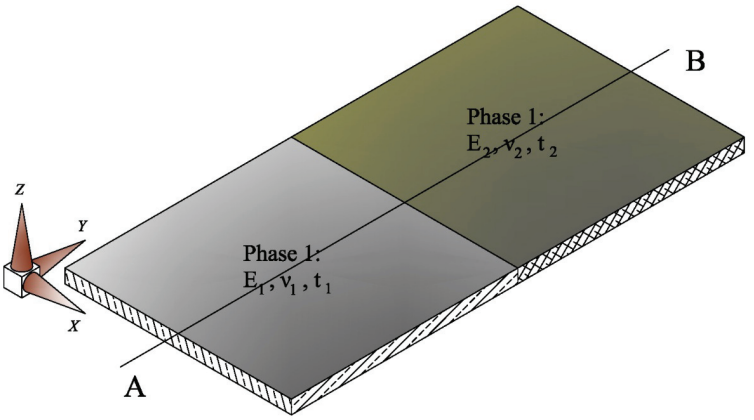

Figure 11: Bi-material plate subjected to uniformly distributed load

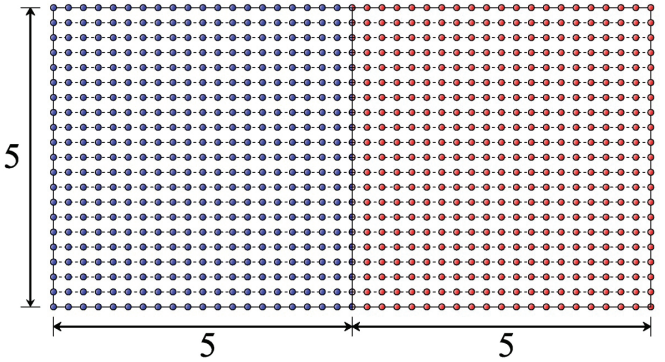

Figure 12: Discretisation scheme for the bi-material plate using separate meshes for each phase

and the elastic modulus of the second phase for each set of analyses is determined from the ratios E_1/E_2 = 1, 2, 3, 5 and 10. The results obtained for the deflection and stress components S_{xx} along the line AB and for each case using the aforementioned ratios are presented in Fig. 13 for the SFSM and obtained results via RKM-FSM are presented in Fig. 14.

The presented results clearly depict that both methods are able to accurately produce the deflections and the stress component S_{xx} along the chosen line. As it was expected, the discontinuity in material properties results in a jump in stress component S_{xx}, while the deflection remains continuous. By using augmented collocation method, both methods have efficiently and accurately captured the jump in stress

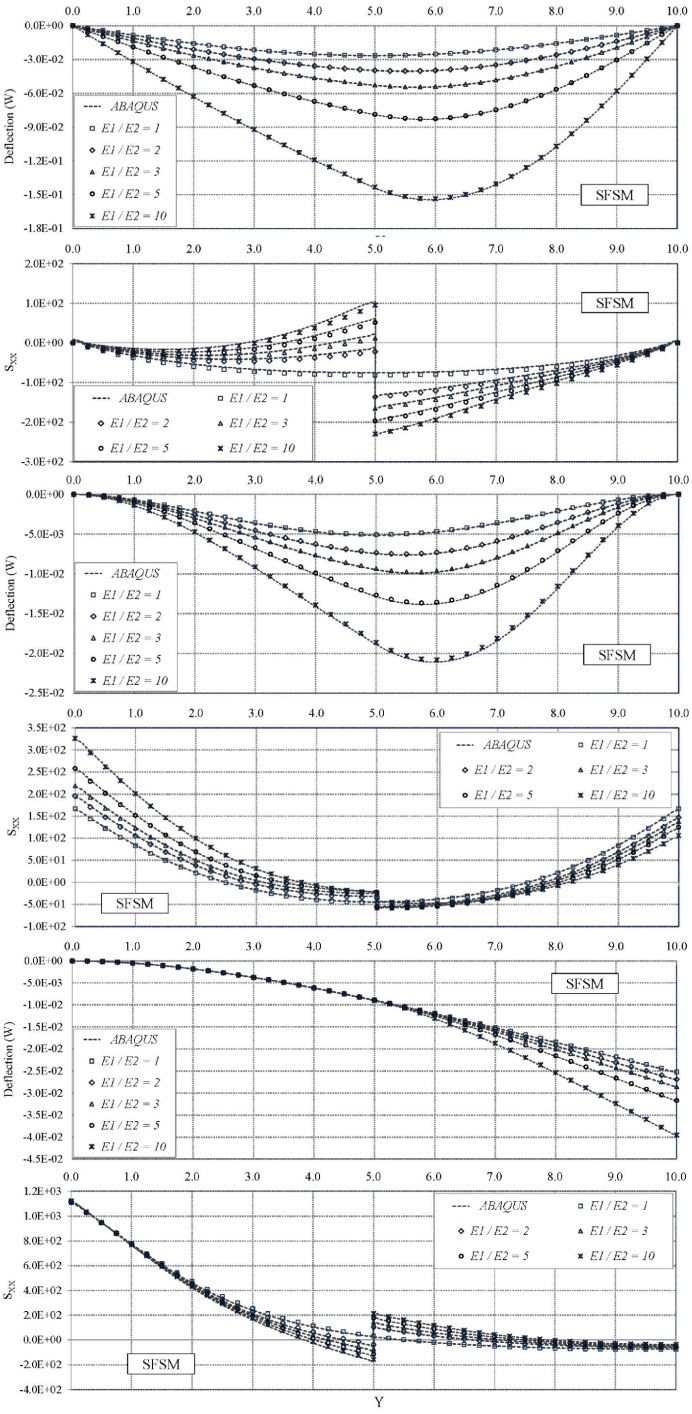

Figure 13: Deflections (w) and stress component S_{XX} along the line AB obtained using SFSM

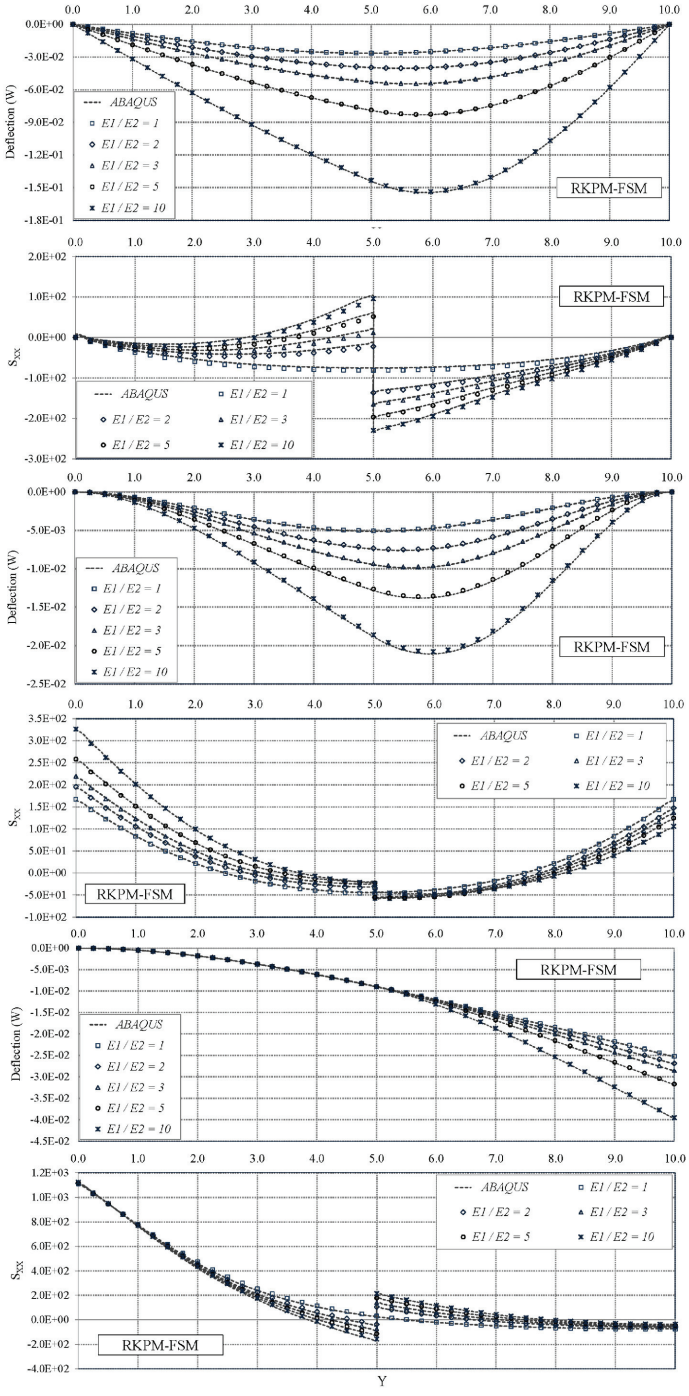

Figure 14: Deflections (w) and stress component S_{XX} along the line AB obtained using RKPM-FSM

across the interface and it is evident that the application of this methodology has eliminated the common fluctuation in field results near the interface which are due to the Gibb's phenomenon [Gutkowski, Chen, and Puckett (1991)].

7 Concluding remarks

This paper has proposed a novel, accurate and versatile meshfree-based FSM in which the capabilities of the generalised RKPM have been incorporated in the FSM. The proposed method has then been utilised for the bending analysis of thin plates and the robustness, accuracy and convergence rate of the proposed method has been demonstrated using a series of standard and challenging numerical examples. The method presented has considerable advantages over the conventional SFSM. Direct inclusion of additional DOFs facilitates method's application in problems with complex boundary conditions, and in this approach boundary conditions can be enforced in algorithmic manner and the need for cumbersome procedures of the amendment of spline functions in the longitudinal direction is eliminated. Moreover, since a complete set of generalised RKPM shape function are used, the particle configuration in the longitudinal direction has more flexibility and unlike the conventional SFSM, particles can be spaced unequally in any desired pattern. This feature allows for the refinement of the particle configuration in the vicinity of areas, which have steep gradients or influencing local effects. Furthermore, the RKP-FSM still retains most of the advantages of the conventional SFSM, such as simplicity and efficiency. The solution presented for treatment of material discontinuity in a bi-material plate is an example of the high potential of the presented methodology in solving much more complex plate problems.

Acknowledgement: A grateful acknowledgement is extended to the School of Civil and Environmental Engineering at the University of New South Wales for providing the first author with a partial scholarship. The authors are thankful to Mr. Sina Pishva for his help in some of the numerical studies.

References

Atluri, S. N.; Shen, S. (2002a): The Meshless Local Petrov-Galerkin (MLPG) Method, Tech Science Press, New York.

Atluri, S. N.; Shen, S. (2002b): The meshless local Petrov-Galerkin (MLPG) method: A simple & less costly alternative to the ?nite element and boundary element method. *CMES: Computer Modeling in Engineering & Sciences*, vol. 3, pp. 11-52

Atluri, S.; Zhu, T. (1998a): A new meshless Petrov-Galerkin (MLPG) approach

to non-linear problems in computer modeling and simulations. *CMES: Computer Modeling in Engineering & Sciences*, vol. 3, pp. 187–196.

Atluri, S.; Zhu, T. (1998b): A new meshless Petrov-Galerkin (MLPG) approach in computational mechanics. *Comput. Mech.*, vol. 22, pp. 117-127

Atluri, S.; Zhu, T. (2000): The meshless local Petrov-Galerkin approach for solving problems in elasto-staticts. *Comput. Mech.*, vol. 25, pp. 169-179

Azhari, M.; Hoshdar, S. ; Bradford, M. A. (2000): On the use of bubble functions in the local buckling analysis of plate structures by the spline finite method. *Int. J. Numer. Methods Engrg.*, vol. 48, no. 4, pp. 583–593.

Babuška, I.; Melnek, J. M. (1996): The partition of unity finite element method: basic theory and applications.*Comput. Methods Appl. Mech. Eng.*, vol. 139, pp. 289–314.

Behzadan, A.; Shodja, H. M.; Khezri, M. (2011): A unified approach to the mathematical analysis of generalised RKPM, gradient RKPM, and GMLS. *Comput. Methods Appl. Mech. Engrg.*, vol. 200, no. 5-8, pp. 540–576.

Belytschko, T.; Lu, Y. Y.; Gu, L. (1994): Element-free Galerkin methods. *Int. J. Numer. Methods Eng.*, vol. 37, pp. 229–256.

Burgess, G.; Mahajerin, E. (1985): A numerical method for laterally loaded thin plates. *Comput. Methods Appl. Mech. Engrg.*, vol. 49, pp. 1–15.

Chen, J. S.; Pan, C.; Wu, C. T.; Liu, W. K. (1996): Reproducing kernel particle methods for large deformation analysis of non-linear structures. *Comput. Methods Appl. Mech. Engrg.*, vol. 139, pp. 195–227.

Chen, J. S.; Wang, H. P. (2000): New boundary condition treatments in meshfree computation of contact problems. *Comput. Methods Appl. Mech. Engrg.*, vol. 187, pp. 441–468.

Cheung, Y. K. (1968): The finite strip method in analysis of elastic plates with two opposite simply-supported ends .In: *Proceeding of institute of civil engineers*, vol. 40, pp. 1-7.

Cheung, Y. K.; Au, F. T. K.; Zhang, D. Y. (1998): Analysis of deep beams and shear walls by finite strip method with C^0 continuous displacement functions. *Thin-Walled Struct.*, vol. 32, pp. 289-303.

Cheung, Y. K.; Au, F. T. K.; Zhang, D. Y. (2000): Finite strip method for free vibration and buckling analysis of plates with abrupt changes in thickness and complex support conditions. *Thin-Walled Struct.*, vol. 36, pp. 89-100.

Cheung, M. S.; Li, W.; Chiadiac, S. E. (1996): Finite strip analysis of bridges. E & FN SPON, London.

Cordes, L. W.; Moran B. (1996): Treatment of material discontinuity in the Element-Free Galerkin method. *Comput. Methods Appl. Mech. Engrg.*, vol. 139, pp. 75-89.

Dawe, D. J.; Wang, S. (1992): Vibration of shear-deformable beams using a spline-function approach. *Int. J. Numer. Meth. Engng.*, vol. 33, pp. 819–844.

Dawe, D. J.; Tan, D. (1999): Finite strip buckling and free vibration analysis of stepped rectangular composite laminated plates. *Int. J. Numer. Meth. Engng.*, vol. 46, pp. 1313–1334.

Dawe, D. J.; Tan, D. (2002): Vibration and buckling of prismatic plate structures having intermediate supports and step thickness changes. *Comput. Methods Appl. Mech. Engrg.*, vol. 191, pp. 2759–2784.

Donning, B. M.; Liu, W. K. (1998): Meshless methods for shear-deformable beams and plates. *Comp. Method. M.*, vol. 152, no. 1-2, pp. 47–71.

Duarte, C. A.; Oden, J. T. (1996): An $h-p$ adaptive method using clouds. *Comput. Methods Appl. Mech. Eng.*, vol. 139, pp. 237–262.

Erkmen, R.E.; Bradford, M.A. (2011a): Treatment of slip locking for displacement-based finite element analysis of composite beam-columns. *Int. J. Numer. Meth. Engrg.,* vol. 85, no. 7, pp. 805-826.

Erkmen, R.E.; Bradford, M.A. (2011b): Coupling of finite element and mesh-free methods for locking-free analysis of shear-deformable beams and plates. *Eng. Comps.,* vol. 28, no. 8, pp. 1003-1027.

Fan, S. C. (1982): Spline finite strip in structural analysis. PhD thesis, University of Hong Kong.

Gutkowski, R. M.; Chen, C. J.; Puckett, J. A. (1991): Plate Bending Analysis by Unequally spaced splines. *Thin-Walled Struct.*, vol. 11, pp. 409–430.

Han, W.; Meng, X. (2001): Error analysis of the reproducing kernel particle method. *Comput. Methods Appl. Mech. Engrg.*, vol. 190, pp. 6157–6181.

Hashemian, A.; Shodja, H. M. (2008): Gradient reproducing kernel particle method. *J Mech. Mater. Struct.*., vol. 3, no. 1, pp. 127–152.

Kawashima, T.; Noguchi, H. (2000): Mesh free analyses of structures with discontinuous field using EFGM. *Trans. JSME (Category-A) in Japanese*, vol. 66, pp. 1786-1793.

Khezri, M.; Hashemian, A.; Shodja H. M. (2009): Analysis of a crack problem via RKPM and GRKPM and a note on particle volume. *ICCES: International Conference on Computational & Experimental Engineering and Sciences*, vol. 11, no. 4, pp. 99–108.

Krongauz, B.; Belytschko, T. (1998): EFG approximation with discontinuous derivatives. *Int. J. Numer. Meth. Engng*., vol. 41, pp. 1215-1233.

Lancaster, P.; Salkauskas, K. (1981): Surfaces generated by moving least squares method. *Math. Comput.*, vol. 37, pp. 141–158.

Lau, S. C. W.; Hancock, G. J. (1996): Buckling of thin-walled structures by a spline finite strip method. *Thin-Walled Struct.* , vol. 4, pp. 269–294.

Levy, M. (1899): Memoire sur la theorie des plaques elastiques planes. *J. Math. Pures. Appl.,* vol. 3, pp. 219.

Li, Q.; Shen, S.; Han, Z. D.; Atluri, S. N. (2003): Application of Meshless Local Petrov-Galerkin (MLPG) to problems with singularities, and material discontinuities, in 3-D elasticity. *CMES: Computer Modeling in Engineering & Sciences*, vol. 4, no. 5, pp. 571–585.

Liew, K. M.; Zou, G. P.; Rajendran, S. (2003): A spline strip kernel particle method and its application to two-dimensional elasticity problems. *Int. J. Numer. Meth. Engng.*, vol. 57, pp. 599–616.

Liu, G. R.; Gu, Y. T. (2005): An introduction to meshfree methods and their programming. Springer, Dordrecht, the Netherlands.

Liu, W. K.; Jun, S.; Li, S.; Adee, J.; Belytschkoo, T. (1995): Reproducing kernel particle methods for structural dynamics. *Int. J. Numer. Meth. Engng.*, vol. 38, pp. 1655–1679.

Lucy, L. B. (1977): A numerical approach to the testing of the fission hypothesis. *Astron. J.*, vol. 82, pp. 1013–1024.

Masuda, S.; Noguchi, H. (2006): Analysis of structure with material interface by meshfree method. *CMES: Computer Modeling in Engineering & Sciences*, vol. 11, no. 3, pp. 131–143.

Nayroles, B.; Touzot, G.; Villon P. (1992): Generalizing the finite element method: diffuse approximation and diffuse elements. *Comput. Mech.*, vol. 10, pp. 307–318.

Pelosi, G. (2007): The finite-element method, Part I: R. L. Courant. *IEEE Antennas Propag.*, vol. 49, no. 2, pp. 180–182.

Shodja, H. M.; Hashemian, A. (2007): A remedy to gradient type constraint dilemma encountered in RKPM. *Adv. Eng. Softw.*, vol. 38, no. 4, pp. 229–243.

Shodja, H. M.; Khezri, M.; Hashemian, A.; Behzadan, A. (2010): RKPM with Augmented Corrected Collocation Method for Treatment of Material Discontinuities. *CMES: Computer Modeling in Engineering & Sciences*, vol. 62, no. 2, pp. 171–204.

Szilard, R. (2004): Theory and Applications of Plate Analysis. John Wiley &

Sons, New Jersey.

Ventsel, E.; Krauthammer, T. (2001): Thin plates and shells: Theory, analysis, and applications. Marcel Dekker, New York.

Vrcelj, Z. ; Bradford, M. A. (2008): A simple method for the inclusion of external and internal supports in the spline finite strip method (SFSM) of buckling analysis. *J. Comput. Struct.*, vol. 86, pp. 529–544.

Vrcelj, Z. ; Bradford, M. A. (2010): On using Legendre polynomials and amended spline transformations in the SFSM for buckling and free vibrations of plates and thin-walled beams. *Thin-Walled Struct.*, vol. 48, no. 10-11, pp. 798–805.

Wagner, G. J. ; Liu, W. K. (2000): Application of essential boundary conditions in meshfree-methods: a corrected collocation method. *Int. J. Numer. Methods Engrg*, vol. 47, no., pp. 1367–1379.

Wittrick, W.H.; Williams, F.W. (1972): Buckling and vibration of anisotropic or isotropic plate assemblies under Combined Loadings. *Int. J. Mech. Sci*, vol. 16, pp. 209-239.

Zhu, T.; Zhang, J. D.; Atluri, S. N. (1998a): A local boundary integral equation (LBIE) method in computational mechanics, and a meshless discretization approach. *Comput. Mech.*, vol. 21, pp. 223-235

Zhu, T.; Zhang, J. D.; Atluri, S. N. (1998b): A meshless local boundary integral equation (LBIE) method for solving non-linear problems. *Comput. Mech.*, vol. 22, pp. 174-186